Contemporary Engineering Sciences, Vol. 8, 2015, no. 20, 943 - 954
HIKARI Ltd, www.m-hikari.com
http://dx.doi.org/10.12988/ces.2015.58229

Influences of Mechanical and Thermal Properties on the Thermoelastic Characteristics in Real Size Cylindrical Thermal Barrier Coatings

Jaegwi Go

Department of Mathematics, Changwon National University
20 Changwondaehak-ro Uichang-gu, Changwon, Gyeongnam 641-773, Korea

Je-Hyun Lee

School of Nano and Advanced Materials Engineering
Changwon National University
20 Changwondaehak-ro Uichang-gu, Changwon, Gyeongnam 641-773, Korea

Seokmin Joo

Electrical Engineering, Gimhae College
198, Saman-ro 112 gil, Gimhae-si, Gyeongnam 50811, Korea

Abstract

Real size cylindrical thermal barrier coating (TBC) models, subjecting to symmetric temperature distribution to the radial direction, were taken into consideration in order to evaluate thermoelastic behaviors such as temperature distribution, displacement, and thermal stresses. Heat flux at each layer interface is adjusted to display temperature distribution profiles and the governing differential equations were derived based on thermoelastic theories. The variation of the ratio between the top coat and the substrate yields deep influence on the thermoelastic characteristics of the cylindrical TBC models. The temperature distribution profiles corresponded closely and more sensitive to the change of k of the top coat than the ratio of k_2/k_1 value. The thermoelastic characteristics in the cylinder react sensitively to the variation of three representative parameters. The ratios of mechanical and thermal properties between the top and bond coats, and between the top coat and substrate are crucial factors to be considered in controlling the thermoelastic behaviors of the TBCs, which can be estimated though mathematical approaches.

Keywords: Layer thickness, Thermal barrier coating, Plasma spraying, Thermoelasticity

1 Introduction

Plasma-sprayed thermal barrier coating (TBC) techniques are widely used in industrial applications such as gas turbines and diesel engines to protect and insulate hot-section metal components [1, 2]. TBC system consists of three primary layers: a ceramic top coat, a superalloy substrate, a metallic bond coat between the substrate and the top coat. In general, TBC failure mechanisms develop due to the mismatch of mechanical and thermal properties at the interface between the top and bond coats, as the TBC system applies to a high operating temperature and cools down to the ambient resulting in the extremely large thermal and residual stresses, respectively [3-5].
Thermal conductivity plays a critical role in controlling heat transfer, and the differences in shape, orientation and distribution of their porosity yield the differences in the thermal conductivity [6-7]. As CTEs are to describe the shrinkage and expansion of material with temperature, the thermodynamic properties and failure mechanisms of composite materials are sensitive to the variation of CTEs [8, 9]. Elastic modulus is the mathematical description for the tendency of an object, subjecting to a loading, to be deformed elastically. Usually, the top coat in the TBC system is always exposed to separation from the bond coat, which is a final phenomenon of typical failure scenario. Owing to the disharmony of elastic modulus between the top and bond coats, a concomitant increases in the mechanical properties with the increase of the number interfaces, providing profound influence in the stresses with the change of elastic modulus [10-12]. Therefore, the analysis of some representative properties, such as layer thickness, thermal conductivity, the coefficient of thermal expansions (CTEs), and elastic modulus, is essential to control the thermoelastic characteristics of TBCs.

However, the study on the thermoelastic characteristics of TBCs with the variation of layer thickness, elastic modulus, thermal conductivity, and CTEs is rare and changeling areas. In this paper, the effects of the thermal and mechanical properties the thermoelastic characteristics investigated for the real cylindrical TBC models based on mathematical approaches. Real size combustion liner with the cylinder shape of 232 mm diameter and 910 mm length was chosen as the real object subjecting to the symmetric temperature load of 1100–950 ℃. The results and the analysis performed here contribute further understanding to the behaviors of TBCs.

2 Mathematical Modelling

2.1. Thermoelastic formulation

Based on the assumption that cylinder is subjecting to symmetric temperature, as shown in Figure 1, distribution equilibrium equation in polar coordinates can be expressed as

$$\frac{\partial \sigma_r}{\partial r} + \frac{\sigma_r - \sigma_\theta}{r} = 0 \qquad (1)$$

where σ_r and σ_θ are radial and circumference stress, respectively.

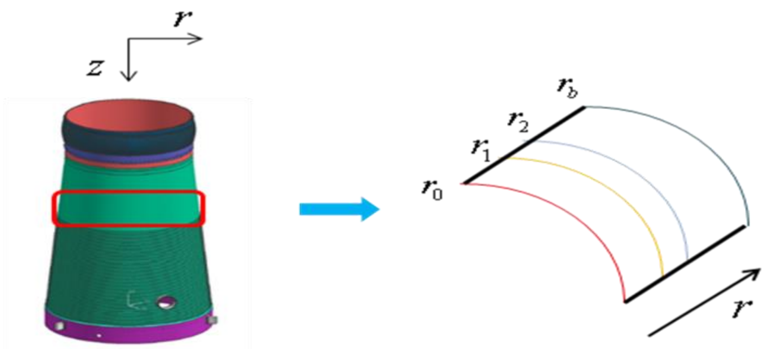

Figure 1. Schematic diagrams of real size cylindrical TBC models.

Since the stresses are associated with the elastic strain, the components of strain due to the thermal expansion are written by

$$\varepsilon_r = \frac{1}{E}\left[\sigma_r - \nu\sigma_\theta\right] + \alpha T$$
$$\varepsilon_\theta = \frac{1}{E}\left[\sigma_\theta - \nu\sigma_r\right] + \alpha T \qquad (2)$$

where ν is the Poisson's ratio, E is the Young's modulus, and α is the coefficient thermal expansion, and ε_r and ε_θ are radial and circumference strain, respectively. Further, the strain-displacement relations for symmetric case are given by

$$\varepsilon_r = \frac{\partial u}{\partial r}$$
$$\varepsilon_\theta = \frac{u}{r}, \qquad (3)$$

where u is the displacement in radial direction. By making use of Eqs. (1)-(3) into the equilibrium equations in two dimensional polar coordinate system, the derived governing equation is

$$\frac{d^2u}{dr^2}+\frac{1}{r}\frac{du}{dr}-\frac{u}{r^2}=(1+\nu)\alpha r\frac{dT}{dr}\,. \tag{4}$$

The analytic solution to the differential Eq (4) is

$$u(r)=(1+\nu)\alpha\frac{1}{r}\int_{r_0}^{r}T(r)rdr+c_1r+\frac{c_2}{r}\,, \tag{5}$$

where c_1 and c_2 are integral constants. With the following boundary conditions

$\sigma_r(r_0)=P_s\,,\qquad \sigma_r(r_b)=P_b\,,$

the integral constants are

$$c_1=\frac{1-\nu}{r_0^2-r_b^2}\left[\frac{P_sr_0^2-P_br_b^2}{E}-\alpha\int_{r_0}^{r_b}T(r)rdr\right],$$

$$c_2=\frac{r_0^2r_b^2(1+\nu)}{r_0^2-r_b^2}\left[\frac{P_s-P_b}{E}-\frac{\alpha}{r_b^2}\int_{r_0}^{r_b}T(r)rdr\right].$$

The solution for the displacement distribution profiles at i th layer is

$$\begin{aligned}u_i(r)&=\frac{r_{i-1}^2[r^2(1-\nu_i)+r_i^2(1+\nu_i)]}{rE_i(r_{i-1}^2-r_i^2)}P_{i-1}+\frac{-r_i^2[r^2(1-\nu_i)+r_{i-1}^2(1+\nu_i)]}{rE_i(r_{i-1}^2-r_i^2)}P_i\\&+\frac{-r^2(1-\nu_i)-r_{i-1}^2(1+\nu_i)}{r(r_{i-1}^2-r_i^2)}\alpha_i\int_{r_{i-1}}^{r_i}T_i(r)rdr+\frac{1+\nu_i}{r}\alpha_i\int_{r_{i-1}}^{r}T_i(r)rdr\end{aligned}, \tag{6(a)}$$

and the solution for the radial distribution profiles at i th layer is

$$\begin{aligned}\sigma_{ri}(r)&=-\frac{E_i}{r^2}\alpha_i\int_{r_{i-1}}^{r}T_i(r)rdr+\frac{E_i(r_{i-1}^2-r^2)}{r^2(r_{i-1}^2-r_i^2)}\alpha_i\int_{r_{i-1}}^{r_i}T_i(r)rdr\\&+\frac{1}{r^2(r_{i-1}^2-r_i^2)}[P_{i-1}r_{i-1}^2(r^2-r_i^2)+P_ir_i^2(r_{i-1}^2-r^2)]\end{aligned}. \tag{6(b)}$$

2.2. Temperature distribution formulation

The governing partial differential equation for the temperature distribution of the cylinder model is, in steady state,

$$\frac{1}{r}\frac{\partial}{\partial r}\left(r\frac{\partial T}{\partial r}\right)+\frac{\partial^2T}{\partial z^2}=0\,. \tag{7}$$

The Eq. (7) is derived based on the assumption that a symmetric temperature is loading to the radial (r) direction (see Fig. 1). The general solution of the Eq. (7) is

$$T(r,z)=d_1J_*(\sqrt{\lambda}r)e^{-\sqrt{\lambda}z}+d_2Y_*(\sqrt{\lambda}r)e^{-\sqrt{\lambda}z}\,, \tag{8}$$

where J_* and Y_* are Bessel functions of order $*$, λ is unknown scalar, and d_1 and d_2 will be determined accorting to the boundary conditions. The boundary conditions for differential constants are given by, at the fixed point $z = z_0$,

$T(r_0, z_0) = T_{in}$, $\quad T(r_1, z_0) = T_1$, $\quad T(r_2, z_0) = T_2$, $\quad T(r_b, z_0) = T_{out}$.

However, only two boundary contions T_{in} and T_{out} are provided and the intergral constants for each layer need to be determined. Additional necessary information thus is required to obtain the unique temperature distribution profile for each layer. Heat flux point takes into account at each layer, and the equations for i^{th} layer are expressed as

$$q_i = \frac{k_i}{L_i}(T_{i-1} - T_i), \quad q_i = q_{i+1}, \tag{9}$$

where q_i is the heat flux into i^{th} layer, k_i the condcutivity, and L_i the length of i^{th} layer. Then, the integral constants for the temperature distribution profile at each i^{th} layer in the cyclinder model can be determined uniquely by solving the following linear system:

$$\begin{aligned}
& d_{i1}J_0(\sqrt{\lambda}r_{i-1}) + d_{i2}Y_0(\sqrt{\lambda}r_{i-1}) = T_{i-1} \\
& d_{i1}J_0(\sqrt{\lambda}r_i) + d_{i2}Y_0(\sqrt{\lambda}r_i) - T_i = 0 \\
& q_i = \frac{k_i}{L_i}(T_{i-1} - T_i), \quad q_i = q_{i+1} \\
& \qquad\qquad \vdots \\
& q_{n-1} = \frac{k_{n-1}}{L_{n-1}}(T_{n-2} - T_{n-1}), \quad q_{n-1} = q_n \\
& q_n - \frac{k_n}{L_n}T_{n-1} = -\frac{k_n}{L_n}T_{out}, \quad i = 1, 2, \cdots, n-1.
\end{aligned} \tag{10}$$

For the cylinder model consisting of n layers, since the T_{i-1} is known value solved by $(i-1)^{th}$ layer linear system and T_{out} is given initial value, the number of $2(n-i)+3$ equations will determine $2(n-i)+3$'s unknown coefficients. When $i = n$, only two unkown integral coefficients d_{n1} and d_{n2} with two equations will be determined easily. Similar process can apply to the temperature distribution profile of the circular disk.

3. Results and Discussion

Temperature distribution profiles are obtained based on the process in the section 2.2, which are appeared through Figs 2(a) and 3(a). The mechanical and thermal properties used for each layer are shown in Table 1. The following boundary conditions

$\sigma_r(r_0) = P_s = 0$, $\sigma_r(r_b) = P_b = 0$,

are applied to investigate the thermoelastic characteristics of real size cylindrical TBC models.

Material/Properties	Elastic Module (*GPa*) at room temperature	Poisson's ratio	Thermal expansion coefficient($10^{-6}/{}^{o}C$)	Thermal conductivity ($W/m\text{-}{}^{o}C$)
Top coating (204C-NS)	100	0.2	2.5(20 – 1300 ^{o}C)	2.0
Bond coating (AMDRY 962)	200	0.3	14	6.4
Substrate (NIMONIC 263)	221	0.3	11.1(20-100 ^{o}C)	11.7

Table 1. Mechanical and thermal properties

3.1. Layer thickness

The effects of layer thickness are appeared in Figure 2. The temperature distribution profiles display the largest decline at the top coat, which explains the property of the low thermal conductivity of the top coat (see Fig. 2(a)). As the ratio *T/S* between the top coat and the substrate increases the bond coat and the substrate are under the loading of lower temperature. The rate of temperature decrease is getting slower due to the increase of metal concentration to the radial direction, demonstrating that the mathematical approach is reliable and reasonable.

As shown in Figure 2(b), smaller displacement develops along the increase of the ratio *T/S* between the top coat and the substrate. The highest tensile radial stress occurs at the interface between the top and the bond coats, and the intensity increases as the ratio *T/S* (see Fig. 2(c)). The substrate is under the compressive radial stress, and similar behavior appears to the change of the layer thickness. However, different phases develop in the circumferential stress distribution profiles. As the ratio *T/S* increases the intensity of the circumferential stress is getting smaller (see Fig. 2(d)).

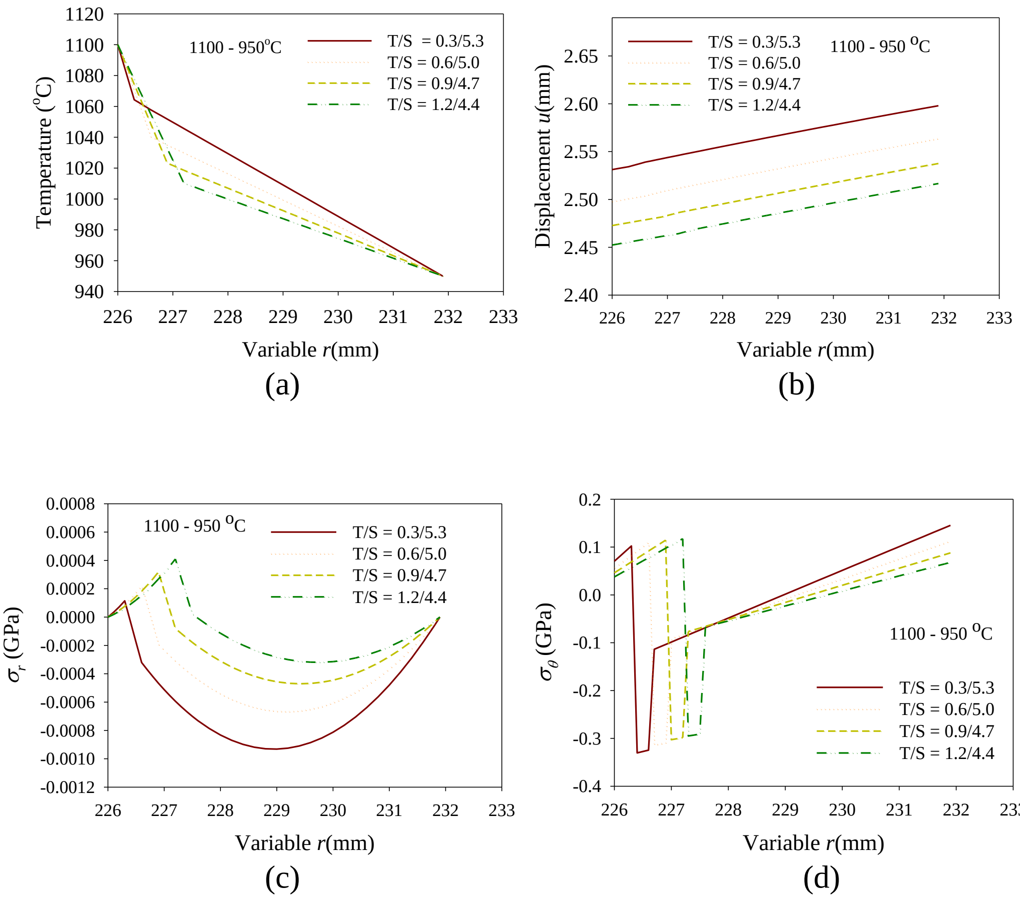

Figure 2. Thermoelastic characteristics with the variation of the ratio *T/S*: (a) temperature, (b) displacement, (c) radial stress, and (d) circumferential stress.

3.2. Thermal conductivity

The effects of thermal conductivity on the thermoelastic characteristics of the cylinder model are introduced through Figure 3. The other material constants used in this study are based on Table 1. Displacement is not proportional to the ratio of k_2/k_1, showing the smallest displacement for the value of $k_2/k_1 = 2/1$ (see Figure 3(b)). In the radial stress, the top coat is exposed to the tensile stress, whereas the bond coat and the substrate are the compressive stress. The interface between the top and bond coats has the maximum tensile stress, and the largest compressive parabolic stress variation is deployed among them at the value of $k_2/k_1 = 11/2$ (see Figure 3(c)). Unlike the radial stress, as shown in Fig. 3(d), the maximum circumferential stress is developed at the bond coat, independent of the ratio of k_2/k_1.

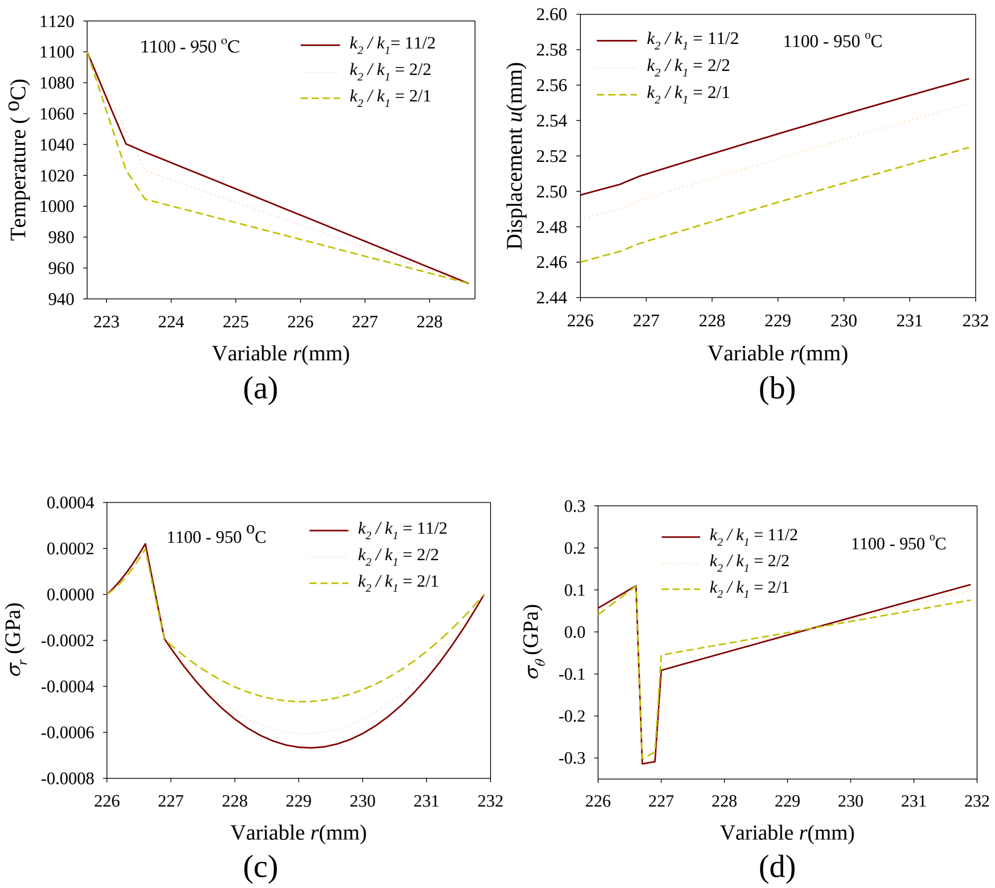

Figure 3. Thermoelastic characteristics with the variation of the ratio k_2/k_1: (a) temperature, (b) displacement, (c) radial stress, and (d) circumferential stress.

3.3. Elastic modulus

Figure 4 exhibits the influences of elastic modulus on the thermoelastic characteristics of the cylinder model. The other material constants used in this study are based on Table 1. The E_2 value of the bond coat is fixed and the E_1 of the top coat is controlled as a variable. Smaller E_1 value generates bigger displacement in the cylinder (see Figure 4(a)). As seen from Figure 4(b), the intensity of the radial tensile stress at the top and bond coats increases when larger E_1 value is applied, showing the maximum tensile stress at the interface between the top and bond coats, and the compressive stress in the substrate is enhanced as the E_1 value decreases. Similar development to the radial stress appears in the circumferential stress of the top coat, with less variation at the bond coat and the substrate (see Figure 4(c)).

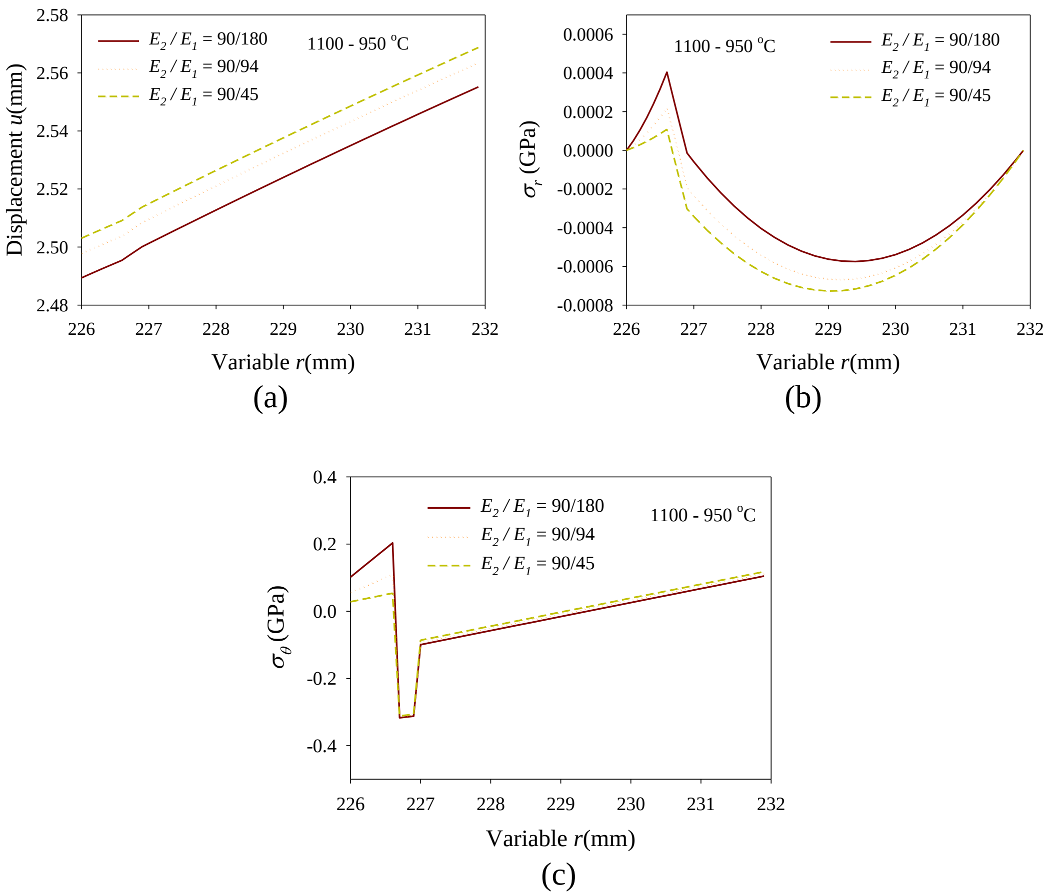

Figure 4. Thermoelastic characteristics with the variation of the ratio E_2/E_1: (a) displacement, (b) radial stress, and (c) circumferential stress.

3.4. Coefficient of thermal expansions

The effects of *CTE* to the thermoelastic characteristics of the cylinder model are investigated and the results are shown in Figure 5. The CTE_1 value of the top coat is changed for the fixed CTE_2 value of the bond coat, and the values shown in Table 1 are used as the other material constants. Displacement increases at the top coat as the CTE_1 value increases, but virtually same in the bond coat and the substrate (see Figure 5(a)). In the radial stress distribution profiles shown in Figure 5(b), the cylinder is under the compressive radial stress for the CTE_1 values of 14 and 20, whereas the tensile radial stress appears for the CTE_1 value of 9.5 at the top coat. The bond coat and the substrate are exposed to the compressive radial stress without any variation with changing the CTE_1 value. Similar development displayed in the circumferential stress distribution profiles, as shown in Figure 5(c). For the CTE_1 values of 14 and 20 the both top and bond coats undergo the compressive stress, while the tensile stress is developed at the top coat for the CTE_1 value of 9.5. The top coat is affected sensitively by the change of the CTE_1 value, showing a same stress state in the bond coat and the substrate.

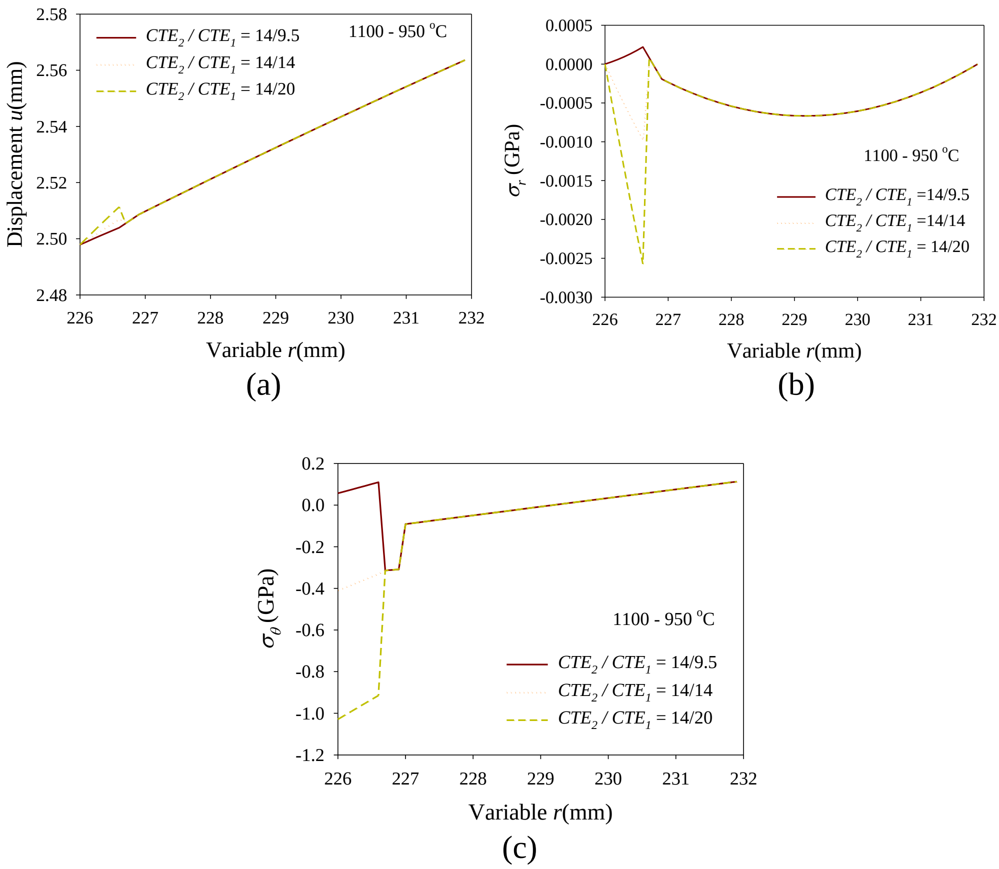

Figure 5. Thermoelastic characteristics with the variation of the ratio CTE_2/CTE_1: (a) displacement, (b) radial stress, and (c) circumferential stress.

4. Conclusion

The thermalelastic characteristics of the cylinder model with influences of various mechanical properties, such as, layer thickness, thermal conductivity k, elastic modulus E, and coefficient of thermal expansions *CTEs* have been investigated based on mathematical approaches. The thermoelastic characteristics of the cylindrical TBC models are susceptible to the variation of the ratio between the top coat and the substrate. The temperature distribution profiles corresponded closely and more sensitive to the change of k of the top coat than the ratio of k_2/k_1 value. The cylinder model displayed larger extension as the ratio of E_2/E_1 increased, whereas smaller extension appeared for larger ratio of CTE_2/CTE_1. The thermoelastic characteristics obtained through mathematical approaches coincided with many experimental results, and the various analyses may be useful to discover technologies for enhancing the thermomechanical properties of TBCs.

Acknowledgements. [1]This research was supported by Basic Science Research Program through the National Research Foundation of Korea (NRF) funded by the Ministry of Education (2013R1A1A2059235). [2]This work was supported by the National Research Foundation of Korea(NRF) grant funded by the Korea government(MSIP) (2011-0030058).

References

[1] R.A. Miller, Oxidation-based model for thermal barrier coating life, *Journal Am. Ceram. Soc.*, **67** (1984), 517-521.
http://dx.doi.org/10.1111/j.1151-2916.1984.tb19162.x

[2] A. Jadhav, N. P. Padture, F. Wu, E. H. Jordan, and M. Gell, Thick ceramic thermal barrier coatings with high durability deposited using solution-precursor plasma spray, *Mater. Sci. and Eng. A*, **405** (2005), 313-320.
http://dx.doi.org/10.1016/j.msea.2005.06.023

[3] D.M. Lipkin and D.R. Clarke, Nondestructive evaluation of the oxidation stresses through thermal barrier coatings using Cr^{3+} piezospectroscopy, *Oxid. Metals*, **45** (1996), 3754-3756.

[4] V.K. Tolpygo and D.R. Clarke, Competition during oxidation between stress generation and relaxation in alumina scales formed by oxidation of a Fe-22Cr-4.8Al-0.3Y alloy, *Oxidation Metals*, **49** (1998), 187-211.

[5] C. Mennicke, E. Schumann, C. Ulrich, and M. Ruehle, Mechanisms controlling the durability of thermal barrier coatings, *Mater. Sci. Forum*, **389** (1997), 251-254.

[6] A. Flores Renteria, B. Saruhan, U. Schulz, H.-J. Raetzer-Scheibe, J. Haug, A. Wiedenmann, Effect of morphology on thermal conductivity of EB-PVD PYSZ TBCs, *Surface & Coatings Technology*, **201** (2006) 2611-2620.
http://dx.doi.org/10.1016/j.surfcoat.2006.05.003

[7] J.R. Nicholls, K.J. Lawson, A. Johnstone, D.S. Rickerby, Methods to reduce the thermal conductivity of EB-PVD TBCs, *Surf. and Coat. Technol.*, **151-152** (2002), 383-391. http://dx.doi.org/10.1016/s0257-8972(01)01651-6

[8] X.W. Wu, R.Y. Luo, Mechanical properties investigation of carbon/carbon composites fabricated by a fast densification process, *Materials Design*, **32** (2011), 2361-2364. http://dx.doi.org/10.1016/j.matdes.2010.11.061

[9] Z.S. Chen, H.J. Li, K.Z. Li, Q.L. Shen, Q.G. Fu, Influence of grain size on wear behavior of SIC coating for carbon/carbon composites at elevated temperatures, *Materials Design*, **53** (2014), 412-418.
http://dx.doi.org/10.1016/j.matdes.2013.07.046

[10] E.S. Puchi-Cabrera, M.H. Staia, A. Iost, A description of the composite elastic modulus of multilayer coated systems, *Thin Solid Films*, **583** (2015), 177-193. http://dx.doi.org/10.1016/j.tsf.2015.02.078

[11] T. Mori,M. Noborisaka, T.Watanabe, T. Suzuki, Oxidation resistance and hardness of TiAlSiN/CrAlYN multilayer films deposited by the arc ion plating method, *Surf. Coat. Technol.*, **213** (2012), 216-220. http://dx.doi.org/10.1016/j.surfcoat.2012.10.050

[12] Z.G. Yuan, J.F. Yang, Z.J. Cheng, X.P. Wang, Q.F. Fang, Preparation and characterization of the Mo(C)N/Mo(C) multilayer coating, *Surf. and Coat. Technol*., **231** (2013) 14-18. http://dx.doi.org/10.1016/j.surfcoat.2012.06.036

Received: August 24, 2015; Published: September 23, 2015